JACS
JOURNAL OF THE AMERICAN CHEMICAL SOCIETY

ARTICLE

pubs.acs.org/JACS

Design, Synthesis, and Traveling Wave Ion Mobility Mass Spectrometry Characterization of Iron(II)− and Ruthenium(II)−Terpyridine Metallomacrocycles

Yi-Tsu Chan,[†,§] Xiaopeng Li,[‡,§] Jing Yu,[†] Gustavo A. Carri,[†] Charles N. Moorefield,[†] George R. Newkome,[*,†,‡] and Chrys Wesdemiotis[*,†,‡]

[†]Departments of Polymer Science and [‡]Chemistry, The University of Akron, Akron, Ohio, 44325, United States

Supporting Information

ABSTRACT: New metallomacrocycles composed of 2,2′:6′,2″-terpyridine (tpy) ligands and Ru^{II} or Fe^{II} transition metal ions were prepared by stepwise directed assembly and characterized by 2D diffusion NMR spectroscopy (DOSY), electrospray ionization traveling wave ion mobility mass spectrometry (ESI TWIM MS), and molecular modeling. The supramolecular polymers synthesized include a homonuclear all-Ru hexamer as well as heteronuclear hexamer and nonamer with alternating Ru/Ru/Fe metal centers. ESI MS yields several charge states from each supramacromolecule. If ESI is interfaced with TWIM MS, overlapping charge states and the isomeric components of an individual charge state are separated based on their unique drift times through the TWIM region. From experimentally measured drift times, collision cross-sections can be deduced. The collision cross-sections obtained for the synthesized supramacromolecules are in good agreement with those predicted by molecular modeling for macrocyclic structures. Similarly, the hydrodynamic radii of the synthesized complexes derived from 2D DOSY NMR experiments agree excellently with the radii calculated for macrocyclic architectures, confirming the ESI TWIM MS finding. ESI TWIM MS and 2D DOSY NMR spectroscopy provide an alternative approach for the structural analysis of supramolecules that are difficult or impossible to crystallize, such as the large macrocyclic assemblies investigated. ESI TWIM MS will be particularly valuable for the characterization of supramolecular assemblies not available in the quantity or purity required for NMR studies.

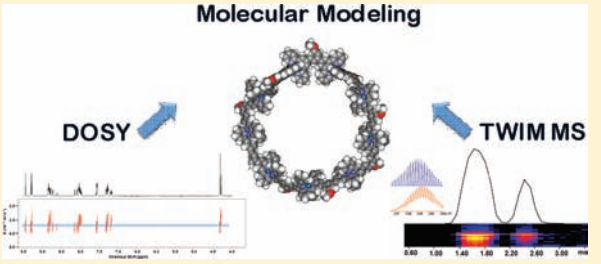

INTRODUCTION

The construction of supramolecular architectures via self-assembly of designed building blocks has experienced significant progress in the past two decades.[1] The elegant work by Lehn,[2−8] Stang,[9−13] Fujita,[14−21] Mirkin,[22−24] and many others[25−29] has demonstrated the importance of metal−ligand coordinative interactions in the formation of such structures. Several successful strategies have been developed for the synthesis of metallocycles with triangular,[30−35] rectangular,[36−41] pentagonal,[42,43] and hexagonal[44−50] shapes. In contrast, only a few larger polygonal structures have been synthesized,[51−56] presumably because their formation is entropically disfavored. Stepwise directed assembly can help to overcome this limitation, as recently shown by Jiang and Lin, who succeeded in constructing a family of larger metallocycles with kinetically inert Pt−alkynyl linkages.[57] Still, the synthesis of predetermined larger metallocycles with rigid spacers remains challenging.

The characterization of large macrocycles poses an additional challenge, because in many cases such substances do not readily form single crystals suitable for X-ray crystallographic analysis. As a result, NMR spectroscopy and electrospray ionization mass spectrometry (ESI MS) have become the principal analytical tools for the determination of metallomacrocyclic structures.[58−63] Under the mild, ambient conditions of ESI, weakly bonded organometallic assemblies available in low quantity can be analyzed intact without the need of extensive sample purification because of the high sensitivity and dispersive nature of MS. This advantage is compromised as the size of an assembly increases, causing the production of isomeric structures with the same masses and charges and, thus, indistinguishable by MS even at high resolution. Moreover, ESI tends to form many, differently charged ions with superimposed isotope clusters from the same macrocycle, which hinders definitive assignment of the correct composition. As recently shown,[50,64−67] these problems can be adequately addressed by interfacing ESI MS with ion mobility spectrometry (IMS),[68−80] which enables mass-, charge-, and shape-dependent dispersion to thereby resolve isomers with distinct architectures as well as deconvolute the isotope clusters of overlapping charge distributions.

IMS and the closely related variant of traveling wave ion mobility mass spectrometry (TWIM MS)[81−83] may be viewed as gas-phase ion chromatography methods, with the ion mobility region being equivalent to the chromatographic column. In the

Received: August 13, 2010
Published: June 30, 2011

dx.doi.org/10.1021/ja107307u | J. Am. Chem. Soc. 2011, 133, 11967–11976

ion mobility region, ions drift under the influence of an electric field against a gas stream. The time needed for an ion to travel through this region is dictated by its mass, charge, and shape and can be converted to a collision cross-section that reflects these critical structural parameters. Comparison of experimental cross-sections with computationally predicted cross-sections obtained for specific architectures, allows for identification of the precise structure and geometry of the particular ions under study. Analogous structure and size information can be obtained by X-ray crystallography and 2D DOSY NMR experiments. Recently, Bowers and co-workers combined drift cell IMS with X-ray data and molecular modeling to characterize Pt-based organometallic assemblies with square, triangular, and prismatic geometries and masses up to ~5800 Da.[66] Here, we report the first combined TWIM MS, molecular modeling, and DOSY NMR investigation on the architectures of new homo- and heteronuclear metallomacrocycles having masses up to ~8500 Da and containing the <tpy−M^{II}−tpy> connectivity, where tpy = 2,2′:6′,2″-terpyridine and M = Fe and Ru. These coordinatively bound supramacromolecules were synthesized by stepwise self-assembly procedures and include larger rings, viz., two hexamers and one nonamer, for which no crystals have yet been obtained. Both the synthesis and the characterization of these novel macromolecules pose significant challenges. Our study examines the agreement between the structures and sizes deduced from the TWIM MS and NMR data to determine whether the MS-based method is as suitable as the already established NMR approach for the analysis of supramolecular architectures. As mentioned above, an MS-based method is much less sensitive to impurities and, hence, would significantly facilitate the characterization of such supramacromolecules.

EXPERIMENTAL SECTION

General Procedures. Reagents and solvents were purchased from Sigma-Aldrich or Fisher. Thin layer chromatography (TLC) was performed on flexible sheets (Baker-flex) precoated with Al_2O_3 (IB-F) or SiO_2 (IB2-F) and visualized by UV light. Column chromatography was conducted using basic Al_2O_3, Brockman Activity I (60−325 mesh), or SiO_2 (60−200 mesh) from Fisher Scientific. UV−vis spectra were recorded on a Chem2000 UV−vis spectrophotometer from Ocean Optics, Inc. ^1H and ^{13}C NMR spectra were recorded on either a Varian NMRS 500 or a Varian Mercury 300 NMR spectrometer at 25 °C; the former instrument was also used to acquire the 2D DOSY NMR spectra. The proteins used to calibrate the drift time scale in TWIM MS experiments, in order to obtain collision cross-sections, were acquired from Sigma-Aldrich. All purchased chemicals were used in the condition received without further purification.

ESI MS and TWIM MS. Electrospray ionization (ESI) mass spectra were acquired with a Waters Synapt HDMS quadrupole/time-of-flight (Q/ToF) tandem mass spectrometer, following procedures described in detail elsewhere.[50] The TWIM MS experiments were performed with the same instrument, using the following parameters (unless noted otherwise): ESI capillary voltage, 1.5 kV; sample cone voltage, 15 V; extraction cone voltage, 3.2 V; desolvation gas flow, 800 L/h (N_2); trap collision energy (CE), 2 eV; transfer CE, 1 eV; trap gas flow, 1.5 mL/min (Ar); ion mobility cell gas flow, 22.7 mL/min (N_2); sample flow rate, 5 μL/min; source temperature, 30 °C; desolvation temperature, 40 °C; IM traveling wave height, 12 V; and IM traveling wave velocity, 350 m/s. The sprayed solution was prepared by dissolving ~0.3 mg of sample in 1 mL of a MeCN/MeOH (1:1, v/v) mixture. Data analyses were conducted using the MassLynx 4.1 and DriftScope 2.1 programs provided by Waters.

Collision Cross-Section Calibration. The drift time scale of the TWIM MS experiments was converted to a collision cross-section scale following the calibration procedure of Scrivens et al.[83] Briefly, the corrected collision cross-sections of the molecular ions of insulin (bovine pancreas), ubiquitin (bovine red blood cells), and cytochrome C (horse heart), obtained from published work,[84,85] were plotted against the corrected drift times (arrival times) of the corresponding molecular ions measured in TWIM MS experiments at the same traveling wave velocity, traveling wave height, and ion mobility gas flow setting used for the metallomacrocycles, viz. 350 m/s, 12 V, and 22.7 mL/min, respectively. All well-characterized conformers observed within each charge state of the calibrants were considered for the construction of the curve.

Molecular Modeling. Energy minimization of the macrocycles and select linear isomers was carried out with the Materials Studio version 4.2 program, using the Anneal and Geometry Optimization tasks in the Forcite module (Accelrys Software, Inc.). The counterions were omitted. An initially energy-minimized structure was subjected to 80−200 annealing cycles with initial and midcycle temperatures of 300 and 1400 K, twenty heating ramps per cycle, one thousand dynamics steps per ramp, and one dynamics step per femtosecond. The temperature vs time dependence of the annealing process is shown in the plot of Figure S7 (Supporting Information). A constant volume/constant energy (NVE) ensemble was used, and the geometry was optimized after each cycle. All geometry optimizations used a universal force field with atom-based summation and cubic spline truncation for both the electrostatic and van der Waals parameters.[65] For each macrocycle and linear structure, 80−200 candidate structures were selected for the calculation of collision cross-sections by the DriftScope 2.1 program, which uses the projection approximation method.[86] Plotting the resulting cross-sections against the corresponding relative energies helps to identify the families of conformers existing for each isomer (Figures S8−S13, Supporting Information). The projection approximation model tends to underestimate the cross-sections, especially of large ions, because it does not treat scattering phenomena properly and neglects long-range interactions between the ions and the gas in the ion mobility region. Therefore, the MOBCAL algorithm[87] was employed to calculate collision cross-sections also by the exact hard sphere scattering[88] and trajectory[89] methods; both account for the details of the scattering process, and the trajectory method also considers long-range ion/gas interactions. In order to keep the computations tractable, the latter two methods were applied to 10−15 structures of each isomer and conformer, selected near the average structures found in the cross-section vs relative energy plots constructed with the projection approximation data (Figures S8−S13). It is worth noting that the Materials Studio program permits geometry optimization and energy minimization for both Fe^{II} as well as Ru^{II} complexes. On the other hand, DriftScope 2.1 and MOBCAL are only parametrized for Fe^{II}; however, because the metal atoms are sequestered by the ligands, and mainly hydrogen atoms on the surface of the complexes interact with the nitrogen gas in the IM cell, the interaction parameters of Fe^{II} can be used to approximate the heavier Ru^{II} centers in DriftScope 2.1 and MOBCAL calculations.

MALDI-ToF Mass Spectrometry. MALDI-ToF MS measurements were performed with a Bruker Ultraflex III ToF/ToF mass spectrometer, equipped with a Nd:YAG laser emitting at a wavelength of 355 nm. All spectra were measured in positive reflector mode.[90] The instrument was calibrated externally with a polystyrene standard prior to each measurement. THF and *trans*-2-[3-(4-*tert*-butylphenyl)-2-methyl-2-propenylidene]malononitrile (DCTB) served as solvent and matrix, respectively. Solutions of the matrix in THF and the macrocycles in MeOH/MeCN (1:1, v/v) were prepared at concentrations of 20 mg/mL and 5 mg/mL, respectively. Sample preparation involved depositing 0.5 μL of matrix solution (20 mg/mL) on the wells of a 384-well ground-steel plate, allowing the spots to dry, depositing 0.5 μL of

Scheme 1. Ru^{II} Hexamer 3 and $[Ru^{II}-Ru^{II}-Fe^{II}]_n$ Macrocycles 4 (n = 2) and 5 (n = 3) Obtained by Self-Assembly of 2[a]

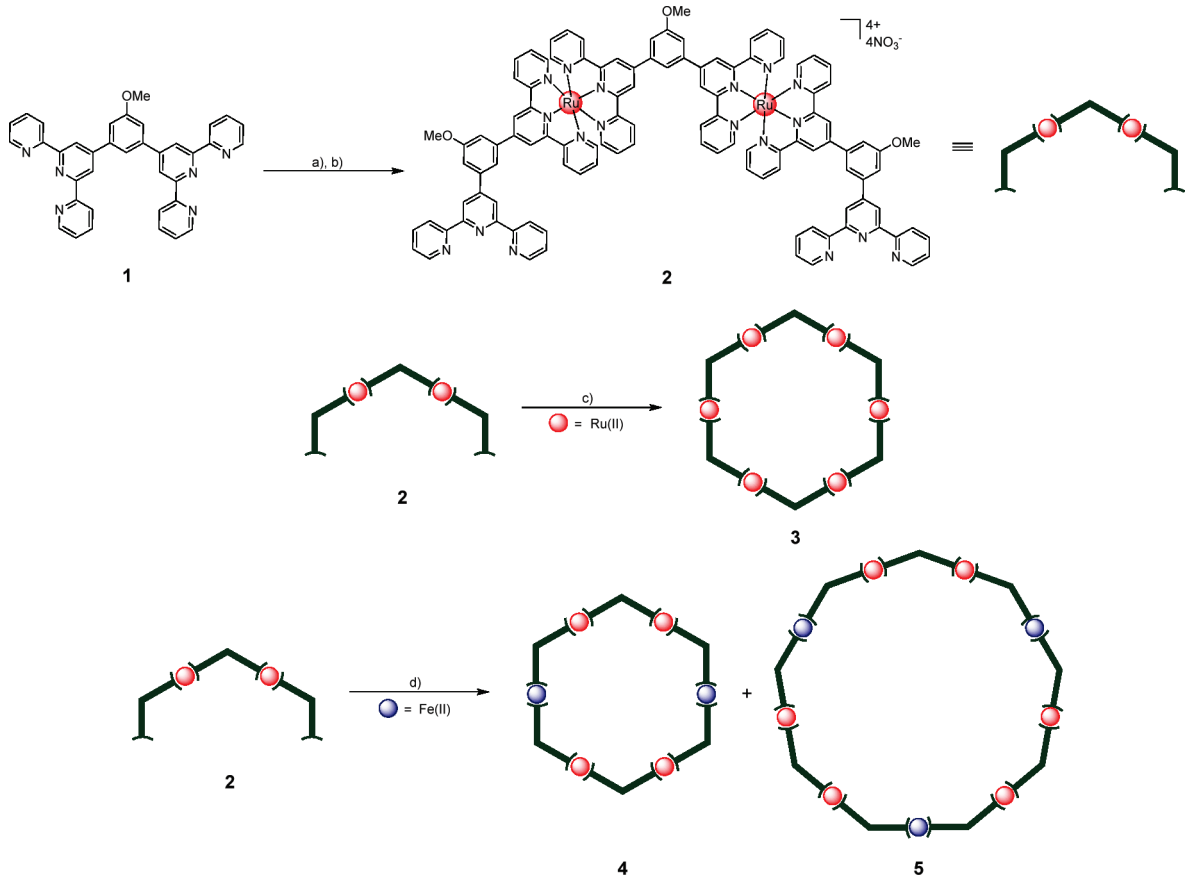

[a] Reagents and conditions: (a) $RuCl_3 \cdot 3H_2O$, EtOH, reflux, 12 h; (b) **1**, *N*-ethylmorpholine, MeOH, reflux, 18 h; (c) $RuCl_2(DMSO)_4$, MeOH, reflux, 2 days; (d) $FeCl_2 \cdot 4H_2O$, MeOH, reflux, 18 h (each macrocycle isolated as the polyPF_6^- salt).

each macrocycle (5 mg/mL) on a spot of dry matrix, and adding another 0.5 μL of DCTB solution on top of the dry macrocycle (sandwich method). Data analyses were conducted with Bruker's flexAnalysis software.

3,5-Di(4′-terpyridinyl)anisole (1). To a stirred solution of 5-methoxyisophthalaldehyde[91] (5.0 g, 30.5 mmol) and 2-acetylpyridine (15.5 g, 127.9 mmol) in EtOH (500 mL) was added a solution of NaOH (6.1 g, 152.5 mmol) in H_2O (15 mL). After the mixture was stirred at 25 °C for 2 h, aqueous NH_4OH (255 mL, 28−30%) was added into the mixture. After the mixture was refluxed for 20 h, the precipitate was filtered, purified by column chromatography (Al_2O_3) using $CHCl_3$ as eluent, and recrystallized from $CHCl_3$/MeOH to give **1**, as a white solid: 4.0 g (23%); mp 242−244 °C; ^{1}H NMR (300 MHz, $CDCl_3$) δ 8.8 (4H, s, Py$H^{3',5'}$), 8.75 (4H, d, J = 4.8 Hz, Py$H^{6,6''}$), 8.70 (4H, d, J = 7.8 Hz, Py$H^{3,3''}$), 7.93−7.87 (5H, m, Py$H^{4,4''}$ and ArH^4), 7.50 (2H, d, J = 1.2 Hz, Ar$H^{2,6}$), 7.39−7.34 (4H, m, Py$H^{5,5''}$), and 4.03 (3H, s, OCH_3); ^{13}C NMR (75 MHz, $CDCl_3$) δ 160.9, 156.5, 156.3, 150.5, 149.4, 141.2, 137.1, 124.1, 121.7, 119.6, 119.3, 113.9, and 56.1; high resolution ESI MS (m/z) 571.2264 $[M + H]^+$ (calcd m/z = 571.2246).

$[Ru_2(1)_3(NO_3)_4]$ (2). Prepared according to literature methods:[46] ^{1}H NMR [500 MHz, $CD_3OD/CDCl_3$ (1:1)] δ 9.46 (4H, s, Py$H^{3',5'}$), 9.31 (4H, s, Py$H^{3',5'}$), 9.01 (4H, d, J = 8.0 Hz, Py$H^{3,3''}$), 8.95 (4H, d, J = 8.0 Hz, Py$H^{3,3''}$), 8.88 (4H, s, free-Py$H^{3',5'}$), 8.75−8.73 (9H, m, ArH^4, free-Py$H^{3,3''}$ and free-Py$H^{6,6''}$), 8.35 (2H, s, ArH^4), 8.05−8.01 (14H, m, Ar$H^{2,6}$, free-Py$H^{4,4''}$ and Py$H^{4,4''}$), 7.91 (2H, s, ArH), 7.77 (2H, s, ArH), 7.61 (4H, d, J = 5.0 Hz, Py$H^{6,6''}$), 7.50 (4H, dd, J = 6.0 Hz, free-Py$H^{5,5''}$), 7.47 (4H, dd, J = 5.5 Hz, Py$H^{6,6''}$), 7.36 (4H, dd, J = 7.0 Hz, Py$H^{5,5''}$), 7.29 (4H, dd, J = 7.0 Hz, Py$H^{5,5''}$), 4.26 (3H, s, OCH_3), and 4.16 (6H, s, OCH_3); ^{13}C NMR [125 MHz, $CD_3OD/CDCl_3$ (1:1)] δ 162.5, 162.4, 159.2, 158.9, 156.9, 156.7, 156.5, 156.3, 153.1, 152.5, 150.5, 149.7, 149.5, 149.4, 142.0, 140.4, 139.5, 139.4, 139.3, 138.7, 129.0, 128.7, 126.3, 125.9, 125.4, 123.2, 123.0, 122.5, 121.1, 119.8, 119.7, 115.9, 115.3, 115.1, 56.7, and 56.5; ESI MS (m/z): 1019.2 $[M - 2NO_3^-]^{2+}$ (calcd m/z = 1019.2), 658.8 $[M - 3NO_3^-]^{3+}$ (calcd m/z = 658.8), and 478.6 $[M - 4NO_3^-]^{4+}$ (calcd m/z = 478.6).

$[Ru_6(1)_6(PF_6)_{12}]$ (3). To a stirred solution of **2** (100.3 mg, 46.4 μmol) in MeOH (800 mL) was added solid $RuCl_2(DMSO)_4$[92] (23.6 mg, 48.7 μmol). After being refluxed for 2 days, the solvent was evaporated in vacuo to give a residue that was purified with column chromatography (SiO_2) using a H_2O/MeCN/sat. $KNO_{3(aq)}$ (1:12.5:1; v/v/v) mixture as eluent; the counterion was subsequently exchanged by adding a slight excess of methanolic NH_4PF_6 (1 M) to yield **3**, as a red solid: 29 mg, 22%; ^{1}H NMR (500 MHz, CD_3CN) δ 9.24 (24H, s, Py$H^{3',5'}$), 8.80 (24H, d, J = 8.0 Hz, Py$H^{3,3''}$), 8.53 (6H, s, ArH^4), 8.03 (12H, s, Ar$H^{2,6}$), 8.00 (24H, dd, J = 8.0 Hz, Py$H^{4,4''}$), 7.54 (24H, d, J = 5.5 Hz, Py$H^{6,6''}$), 7.26 (24H, dd, J = 7.0 Hz, Py$H^{5,5''}$), and 4.28 (18H, s, OCH_3); ^{13}C NMR (125 MHz, CD_3CN) δ 162.7, 159.3, 156.6, 153.6, 148.6, 140.9, 139.2, 128.7, 125.8, 123.2, 121.1, 115.9, and 57.1; ESI MS (m/z) 1297.7 $[M - 4PF_6^-]^{4+}$ (calcd m/z = 1297.6), 1009.1 $[M - 5PF_6^-]^{5+}$ (calcd m/z = 1009.1), 816.7 $[M - 6PF_6^-]^{6+}$ (calcd m/z = 816.8), 679.3 $[M - 7PF_6^-]^{7+}$ (calcd m/z = 679.4), 576.4 $[M - 8PF_6^-]^{8+}$ (calcd m/z = 576.3), 496.2 $[M - 9PF_6^-]^{9+}$ (calcd m/z = 496.2), 432.1 $[M - 10PF_6^-]^{10+}$ (calcd m/z = 432.1), 379.6 $[M - 11PF_6^-]^{11+}$ (calcd m/z = 379.6), and 335.9 $[M - 12PF_6^-]^{12+}$ (calcd m/z = 335.9).

Self-Assembly of 4 and 5. To a stirred solution of **2** (66.4 mg, 30.7 μmol) in MeOH (250 mL) was slowly added a solution of $FeCl_2 \cdot 4H_2O$ (6.4 mg, 32.2 μmol) in MeOH (50 mL). After being

dx.doi.org/10.1021/ja107307u |J. Am. Chem. Soc. 2011, 133, 11967–11976

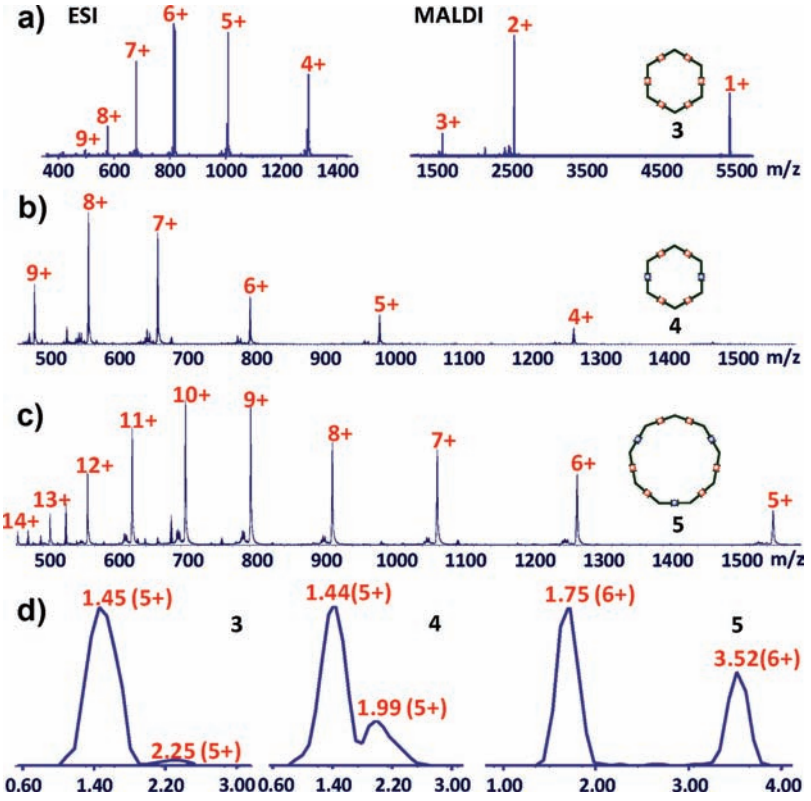

Figure 1. Mass spectra and drift time distributions of **3**, **4**, and **5**. (a) ESI (left) and MALDI (right) mass spectra of **3**. (b) ESI mass spectrum of **4**. (c) ESI mass spectrum of **5**. (d) Drift time distributions for the m/z ratio corresponding to the +5 charge state of **3**, +5 charge state of **4**, and +6 charge state of **5**. The peaks at 1.45 ms, 1.44 ms, and 1.75 ms arise from the cyclic architectures; whereas, those at 2.25 ms, 1.99 ms, and 3.52 ms arise from the corresponding linear isomers. (The minor peaks observed at the low-mass sides of the major peaks mainly arise from the loss of PF_5 from the PF_6^- counterions.[61]).

refluxed for 18 h, the solvent was evaporated in vacuo and the resultant residue was subjected to column chromatography (SiO_2) using a H_2O/MeCN/sat. $KNO_{3(aq)}$ (1:10:1; v/v/v) mixture as eluent to separate macrocycles **4** (R_f = 0.32) and **5** (R_f = 0.22). The NO_3^- counterions were converted to PF_6^- by treating the eluates with an excess of methanolic NH_4PF_6 (1 M).

$[Ru_4Fe_2(1)_6(PF_6)_{12}]$ (4). Yield 42.2 mg, 49%; ^{1}H NMR (500 MHz, CD_3CN) δ 9.42 (8H, s, Py$H^{3',5'}$), 9.28 (8H, s, Py$H^{3',5'}$), 9.25 (8H, s, Py$H^{3',5'}$), 8.83−8.80 (16H, m, Py$H^{3,3''}$), 8.77 (8H, d, J = 8.5 Hz, Py$H^{3,3''}$), 8.64 (4H, s, ArH^4), 8.54 (2H, s, ArH^4), 8.14 (4H, s, ArH), 8.08 (4H, s, ArH), 8.04−7.96 (28H, m, ArH and Py$H^{4,4''}$), 7.55 (16H, d, J = 5.0 Hz, Py$H^{6,6''}$), 7.30 (8H, d, J = 5.0 Hz, Py$H^{6,6''}$), 7.26 (16H, dd, J = 6.5 Hz, Py$H^{5,5''}$), 7.17 (8H, dd, J = 6.5 Hz, Py$H^{5,5''}$), 4.31 (12H, s, OCH_3), and 4.29 (6H, s, OCH_3); ^{13}C NMR (125 MHz, CD_3CN) δ 162.9, 162.8, 161.6, 159.3, 159.2, 156.8, 156.7, 154.2, 153.6, 150.9, 148.7, 141.1, 140.9, 140.8, 140.0, 139.3, 128.8, 128.6, 125.8, 125.1, 123.3, 123.2, 121.3, 121.2, 116.3, 116.1, 116.0, 57.3, and 57.2; ESI MS (m/z) 1275.2 $[M - 4PF_6^-]^{4+}$ (calcd m/z = 1275.1), 991.1 $[M - 5PF_6^-]^{5+}$ (calcd m/z = 991.1), 801.7 $[M - 6PF_6^-]^{6+}$ (calcd m/z = 801.8), 666.5 $[M - 7PF_6^-]^{7+}$ (calcd m/z = 666.5), 565.0 $[M - 8PF_6^-]^{8+}$ (calcd m/z = 565.1), 486.2 $[M - 9PF_6^-]^{9+}$ (calcd m/z = 486.2), 422.9 $[M - 10PF_6^-]^{10+}$ (calcd m/z = 422.9), 371.4 $[M - 11PF_6^-]^{11+}$ (calcd m/z = 371.5), and 328.4 $[M - 12PF_6^-]^{12+}$ (calcd m/z = 328.4).

$[Ru_6Fe_3(1)_9(PF_6)_{18}]$ (5). Yield 12.1 mg, 14%; ^{1}H NMR (500 MHz, CD_3CN) δ 9.44 (12H, s, Py$H^{3',5'}$), 9.30 (12H, s, Py$H^{3',5'}$), 9.27 (12H, s, Py$H^{3',5'}$), 8.85−8.82 (24H, m, Py$H^{3,3''}$), 8.79 (12H, d, J = 8.0 Hz, Py$H^{3,3''}$), 8.72 (6H, s, ArH^4), 8.61 (3H, s, ArH^4), 8.15 (6H, s, ArH), 8.09 (6H, s, ArH), 8.05−7.97 (42H, m, ArH and Py$H^{4,4''}$), 7.56 (24H, d, J = 5.5 Hz, Py$H^{6,6''}$), 7.32 (12H, d, J = 5.5 Hz, Py$H^{6,6''}$), 7.28 (24H, dd, J = 6.5 Hz, Py$H^{5,5''}$), 7.18 (12H, dd, J = 6.5 Hz, Py$H^{5,5''}$), 4.31 (18H, s, OCH_3), and 4.28 (9H, s, OCH_3); ^{13}C NMR (75 MHz, CD_3CN) δ 162.8, 162.7, 161.6, 159.3, 159.2, 156.8, 156.7, 154.2, 153.6, 150.8, 148.6, 141.0, 140.8, 140.7, 140.0, 139.3, 128.8, 128.6, 125.9, 125.1, 123.2, 123.1, 120.8, 120.7, 116.5, 116.3, 116.2, 57.3, and 57.2; ESI MS (m/z) 1558.9 $[M - 5PF_6^-]^{5+}$ (calcd m/z = 1559.0), 1274.9 $[M - 6PF_6^-]^{6+}$ (calcd m/z = 1275.0), 1072.1 $[M - 7PF_6^-]^{7+}$ (calcd m/z = 1072.1), 920.0 $[M - 8PF_6^-]^{8+}$ (calcd m/z = 920.0), 801.7 $[M - 9PF_6^-]^{9+}$ (calcd m/z = 801.7), 706.9 $[M - 10PF_6^-]^{10+}$ (calcd m/z = 707.0), 629.6 $[M - 11PF_6^-]^{11+}$ (calcd m/z = 629.5), 564.8 $[M - 12PF_6^-]^{12+}$ (calcd m/z = 565.0), 510.4 $[M - 13PF_6^-]^{13+}$ (calcd m/z = 510.4), 463.5 $[M - 14PF_6^-]^{14+}$ (calcd m/z = 463.6), 423.1 $[M - 15PF_6^-]^{15+}$ (calcd m/z = 423.1), and 387.6 $[M - 16PF_6^-]^{16+}$ (calcd m/z = 387.6).

RESULTS AND DISCUSSION

The $[Ru_2(1)_3(NO_3)_4]$ trimer **2** was prepared according to our previously reported procedure.[46] The full Ru^{II} hexamer (Scheme 1) was generated by refluxing a dilute solution (5.8×10^{-5} M) of **2** and 1.05 equiv of $RuCl_2(DMSO)_4$[92] in methanol for 2 days. After column chromatography (SiO_2; eluent: H_2O/MeCN/sat. $KNO_{3(aq)}$, 1:12.5:1 v/v/v) and counterion exchange (NO_3^- to PF_6^-), the hexamer **3** was isolated in 22% yield. The ^{1}H NMR spectrum (Figure S1b, Supporting Information) of **3** exhibits four sharp singlets at 9.24 (3′,5′-tpy$H$s), 8.53 (4-ArH), 8.03 (2,6-ArHs), and 4.28 (OCH_3) ppm supporting the presence of the cyclic structure. In comparison with trimer **2** (Figure S1a), an expected upfield shift for 6,6″-tpy$H$s of **3** from 8.74 to 7.54 ppm further confirms that the <tpy−Ru^{II}−tpy> units are

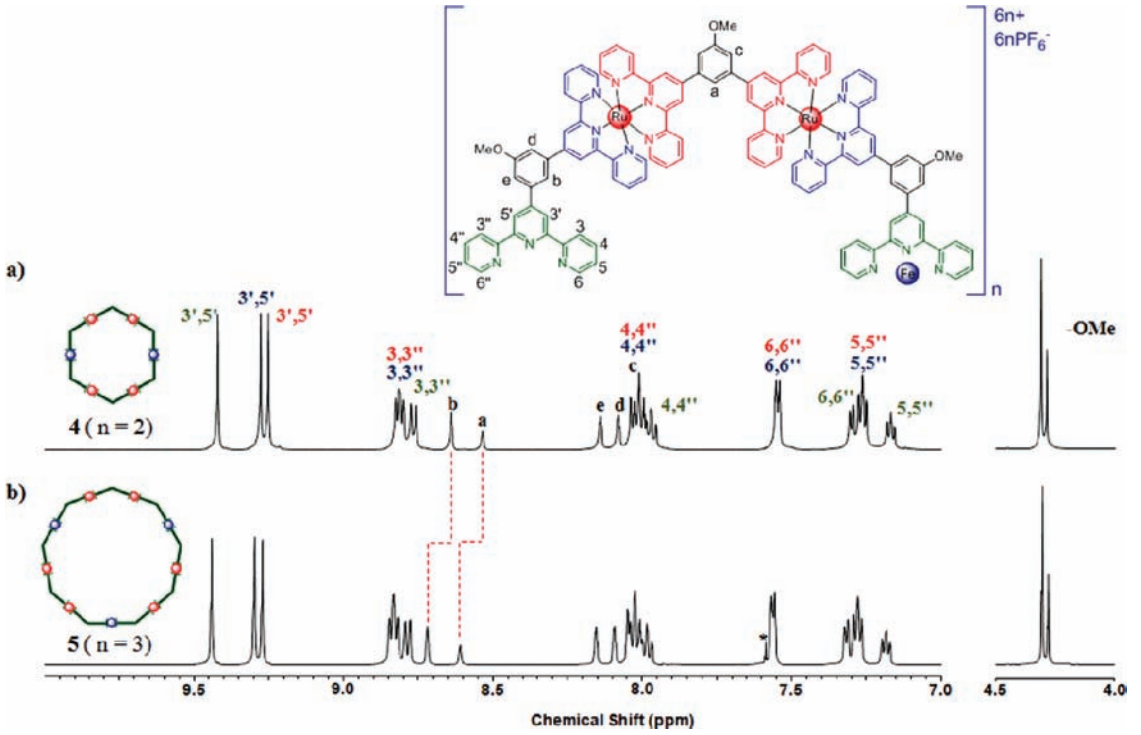

Figure 2. ^{1}H NMR spectra of (a) hexamer **4** and (b) nonamer **5**. The peak marked by * is due to residual $CHCl_3$.

now confined in a macrocycle. The hexagonal motif is further corroborated by the three intense MALDI-ToF MS peaks (Figure 1a, right) at m/z 5625.2 $[M - PF_6^-]^+$ (calcd m/z = 5625.3), 2739.9 $[M - 2PF_6^-]^{2+}$ (calcd m/z = 2739.7), and 1778.3 $[M - 3PF_6^-]^{3+}$ (calcd m/z = 1778.5) and the six intense ESI MS peaks (Figure 1a, left) at m/z 1297.7 $[M - 4PF_6^-]^{4+}$ (calcd m/z = 1297.6), 1009.1 $[M - 5PF_6^-]^{5+}$ (calcd m/z = 1009.1), 816.7 $[M - 6PF_6^-]^{6+}$ (calcd m/z = 816.8), 679.3 $[M - 7PF_6^-]^{7+}$ (calcd m/z = 679.4), 576.4 $[M - 8PF_6^-]^{8+}$ (calcd m/z = 576.3), and 496.2 $[M - 9PF_6^-]^{9+}$ (calcd m/z = 496.2). The isotope patterns of the +1 to +12 charge states (Figure S2, Supporting Information) are in accord with the calculated distributions. It is noteworthy that the intact hexamer **3** could not be detected in a previous MALDI-ToF MS study, which utilized a nitrogen laser.[61] Such lasers emit light of 337 nm, which is strongly absorbed by **3**−**5** (Figure 3; vide infra), leading to their destruction. In contrast, the absorptivity of **3**−**5** at 355 nm, i.e., the wavelength emitted by the currently used Nd:YAG laser, is substantially reduced (vide infra), enabling their observation by MALDI MS. Fragments of the hexamer **3** are essentially absent in both the ESI as well as the MALDI mass spectrum (Figure 1a), in agreement with the high stability of such <tpy−Ru^{II}−tpy> connectivity.[93,94]

Reaction of $[Ru_2(\mathbf{1})_3(NO_3)_4]$ trimer **2** (Scheme 1) with 1.05 equiv of $FeCl_2 \cdot 4H_2O$ in methanol at the reflux temperature for 18 h gave the heteronuclear $[Ru^{II}-Ru^{II}-Fe^{II}]_n$ macrocycles **4** (n = 2, hexamer) and **5** (n = 3, nonamer), which were isolated by column chromatography (SiO_2) using H_2O/MeCN/sat. $KNO_{3(aq)}$ (1:10:1; v/v/v), as eluent; the NO_3^- counterions were exchanged with PF_6^- by adding a slight excess of methanolic NH_4PF_6 (1 M) to the eluate. After chromatographic purification and counterion exchange, **4** and **5** were obtained in yields of 49% and 14%, respectively. The ^{1}H NMR spectrum of

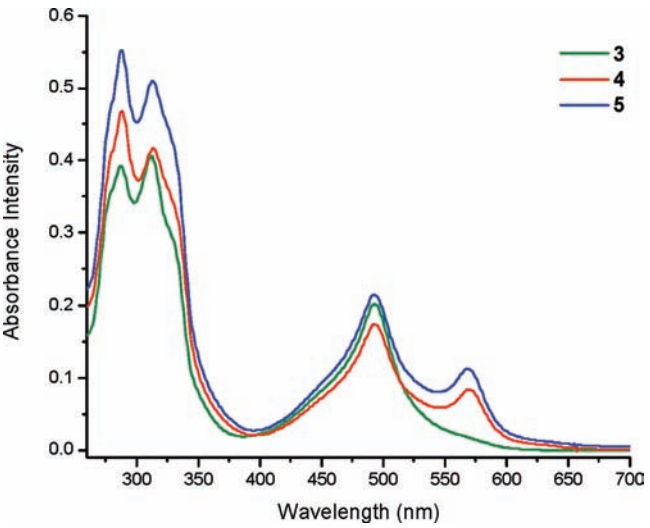

Figure 3. Absorption spectra of macrocycles **3**, **4**, and **5** in dilute MeCN (1.0×10^{-6} M).

macrocycle **4** (Figure 2a) reveals three types of 3′,5′-tpy*H*s (δ = 9.42, 9.28, and 9.25 ppm) and two distinct singlets at 4.31 and 4.29 ppm in a 2:1 ratio for the methoxy groups bordered by Ru/Fe and Ru/Ru, respectively. The $[Ru^{II}-Ru^{II}-Fe^{II}]_2$ sequence in the cyclic structure also leads to five different singlets at 8.64 (b-Ar*H*), 8.54 (a-Ar*H*), 8.14 (e-Ar*H*), 8.08 (d-Ar*H*), and 8.04 (c-Ar*H*), which are confirmed by the weak meta couplings in the 2D COSY NMR spectrum (Figure S3, Supporting Information). The ^{1}H NMR spectrum of nonamer **5** (Figure 2b) exhibits a similar pattern, but the signals of the terpyridine part show a slight downfield shift relative to the corresponding signals in **4**, presumably because the extra metal centers in the larger ring

result in added electron deficiency; moreover, in comparison with hexamer **4**, the benzene rings of nonamer **5** have more conformational flexibility to avoid the shielding effect provided by the adjacent pyridines, which causes its inner aromatic protons (a- and b-Ar*H*s in Figure 2) to shift further downfield ($\Delta\delta$ = +0.08 and +0.07 ppm, respectively). The cyclic structure **4** is verified by ESI MS (Figure 1b) with the peaks at m/z 1275.2, 991.1, 801.7, 666.5, 565.0, and 485.8, which agree well with its +4 to +9 charge states, respectively; the corresponding isotope distributions of **4** are shown in Figure S4, Supporting Information. Similarly, the ESI mass spectrum of **5** confirms the nonameric $[Ru^{II}-Ru^{II}-Fe^{II}]_3$ structure with ten intense signals representing multiply charged ions with +5 to +14 charges. Notably, the isotope pattern observed for the highly charged $[M - 16PF_6^-]^{16+}$ ion from nonamer **5** is in good accordance with the theoretical distribution (Figure S5, Supporting Information). MALDI MS was also performed on **4** and **5**, but no intact macrocycles were observed due to the lower stability of <tpy−Fe^{II}−tpy> containing complexes under MALDI conditions.[93,94]

The UV−vis spectra of macrocycles **3**−**5** in dilute MeCN solution (Figure 3 , and Table S1, Supporting Information) exhibit the expected absorption transitions. In the case of **3**, the peaks at 288 and 313 nm are attributed to ligand-centered (LC) absorption and the peak at 494 nm to the metal-to-ligand charge-transfer transition (MLCT) for Ru^{II} complexes.[95] Macrocycles **4** and **5** give rise to the same bands plus the MLCT band of Fe^{II} complexes, which is observed at 568 nm. Increasing the ring size from hexamer **4** to nonamer **5** results in an increase in the molar extinction coefficient of each absorption band (Table S1), consistent with the corresponding increase in the number of ligands and Fe^{II}/Ru^{II} metal centers in **5**.

The $[M - 5PF_6^-]^{5+}$ charge states of **3** and **4** (cf., Figures S2 and S4, respectively) were selected for ion mobility separation due to the low number of possible ligand/metal combinations at their mass-to-charge ratios.[50,65] Two isomers are detected after ion mobility separation for both **3** and **4** (Figure 1d). Numerous IMS and TWIM MS studies have demonstrated that flexible, extended structures drift more slowly during ion mobility separation (due to collisions with the buffer gas) than compact, less flexible architectures.[66−80] Our recent TWIM MS study of self-assembled Cd^{II} macrocycles confirmed this trend.[50] On the basis of these facts, the strong signals with shorter drift times, viz., 1.45 and 1.44 ms, are assigned to the expected cyclic structures and the weak signals with the longer drift times, viz., 2.25 and 1.99 ms, to ring-opened isomers, which might be generated in the ESI process or during ion mobility separation, as they are not observed in the NMR experiments (vide supra). Ion mobility analysis has also been performed on the $[M - 6PF_6^-]^{6+}$ ions from **5**; it yields signals at 1.75 and 3.52 ms (Figure 1d) which, according to the foregoing discussion, must correspond to cyclic and ring-opened isomers, respectively.

Molecular modeling reveals that the hexameric macrocycles **3** and **4** have consistently circular (O-shaped) conformations, while the larger nonameric macrocycle **5** can exist in circular (O-shaped) as well as twisted (8-shaped) conformations, with the former being more probable (Figure S10, Supporting Information). For the linear isomers of **3**−**5**, molecular modeling predicts mainly extended conformations, but there is also a small fraction of compact, ring-like conformers which is most densely populated for the larger complex **5** (see Figures S11−S13, Supporting Information). The chain ends of the compact linear conformers are in close proximity, which should facilitate ring-closure to the thermodynamically more stable macrocyclic isomers. Any remaining compact linear conformers would drift together with the macrocyclic species because of their very similar shapes and, hence, could be present as minor components in the ion populations giving rise to the TWIM signals at 1.45, 1.44, and 1.75 ms.[66]

From the drift times of $[M - 5PF_6^-]^{5+}$ and $[M - 6PF_6^-]^{6+}$, experimental collision cross-sections (CCSs) can be derived by calibrating the drift time scale of our TWIM device, as has been reported.[74,83] The calibration curve (Figure S6) was built by the procedure of Scrivens et al.,[83] using insulin, ubiquitin, and cytochrome C as calibrants; the CCSs of several charge states of these proteins have been established by drift cell IMS.[83−85] The calibration curve constructed (Figure S6) was tested with lysozyme, for which cross-sectional data acquired by drift cell IMS are also available.[85] The cross-sections of lysozyme ions obtained from the calibration curve matched within 2% those measured by conventional IMS (see Supporting Information), indicating that the traveling wave does not induce significant conformational changes in the protein calibrants[96] and that TWIM MS can provide correct cross-sections.

Our calibration curve (Figure S6) leads to the experimental collision cross-section listed in Table 1. The theoretical collision cross-sections obtained by the trajectory method, which treats most rigorously the collision process between ions and buffer gas in the ion mobility region,[97] are included in Table 1. There is fair agreement (within 12−13%) between the experimental and calculated CCSs for the hexameric macrocycles **3** and **4**, as well as between the experimental CCS of the macrocyclic nonamer **5** and the CCS calculated for a mixture of cyclic O-shaped and 8-shaped **5**. The measured values lie, however, consistently below the calculated values (by 12−13%); this difference is attributed to the omission of the PF_6^- counterions in the calculations (vide infra for the reason of the omission). Recent TWIM MS studies on protein complexes[98] and oligosaccharides[99] have provided strong evidence that the addition of counterions to compact (globular) structures leads to increased compactness and decreased collision cross-sections. In the same vein, adding PF_6^- anions to macrocyclic **3**−**5** should promote ring contraction to a more stable structure due to a reduction in like-charge repulsions, resulting from the development of attractive electrostatic interactions between the PF_6^- units and the positive Fe^{II} and/or Ru^{II} centers.

The experimental collision cross-sections of the more slowly drifting, less compact components of **3**−**5** (Table 1) are markedly larger than those of the macrocycles. Particularly large is the difference between the CCSs of linear **5** and cyclic **5**, resulting in a considerable difference in the drift times of these isomers (cf., Figure 1d). The measured collision cross-sections of the less compact components of **3**−**5** are in reasonable agreement (within 3−10%) with the cross-sections predicted by theory for extended linear architectures; nevertheless, the measured CCSs are now consistently higher (by 3−10%) than the calculated CCSs. Also this trend can be accounted for by the omission of counterions in the calculations. The inclusion of counterions in protein complexes has been shown to increase their stabilities and to cause their partially denatured (and, hence, extended) conformations to become more extended;[98] an analogous action by the PF_6^- counterions reconciles the slightly larger CCSs measured for ring-opened **3**−**5** than predicted by theory for linear structures without any PF_6^-.

Table 1. Collision Cross-Sections of Metallomacrocycles 3−5 and Their Linear Isomers

			cross-section (calcd) [Å^2][b]	
complex	drift time (exp) [ms]	cross-section (exp) [Å^2][a]	architecture	TJ
3 (5+)	1.45 cyclic	766	cyclic	874 (16)
	2.25 linear	1038	linear, extended	945 (39)
			linear, compact	804 (22)
4 (5+)	1.44 cyclic	760	cyclic	878 (14)
	1.99 linear	978	linear, extended	950 (34)
			linear, compact	802 (20)
5 (6+)	1.75 cyclic	1081	cyclic, O-shaped	1305 (35)[d]
			cyclic, 8-shaped	1142 (28)[d]
	3.52 linear	1464	linear, extended	1362 (40)
			linear, compact	1191 (44)

[a] Obtained by calibrating the drift time scale of the TWIM device with standards of known cross-sectional data (calibration plot shown in Figure S6).[65] [b] Obtained from the energy-minimized structures deduced computationally using the trajectory (TJ) method of the MOBCAL program (see Experimental Section). The numbers in parentheses are the corresponding standard deviations. See Table S2 for collision cross-sections obtained using the less rigorous projection approximation (PA) and exact hard sphere scattering (EHSS) methods. [d] The average collision cross-section of both macrocyclic architectures is 1224 Å^2.

The forgoing discussion underscores that counteranions can affect subtly, yet measurably, the shapes and collision cross-sections of organometallic supramacromolecules; however, X-ray studies by several groups have documented that they are highly disordered within the crystal lattice and difficult to locate accurately even in relatively small self-assemblies.[2,3,14,15,17,19,30,100] Furthermore, counterions may readily dissociate during the heating process in molecular mechanics/dynamics calculations. For this reason, counterions have generally been omitted in the molecular modeling of supramolecules.[11−13,16] Attempting to position them arbitrarily in the cavities or periphery of **3**−**5** until a structure is found that matches the experimentally observed CCSs is not practical with the sizes of **3**−**5**, which carry seven to twelve counterions in the charge states examined (Table 1). More information about how the PF_6^- anions might affect macrocyclic architectures was therefore sought by a tandem mass spectrometry (MS^2) experiment on triply charged **3**, which contains nine PF_6^- counterions. Collisionally activated dissociation (CAD) of mass-selected **3** causes the consecutive eliminations of PF_5 molecules (cf., Figure S14, Supporting Information); in this process, the PF_6^- counterions (145 Da) are converted to F^- (19 Da). TWIM separation of the fragments[67] shows that they have essentially the same drift time as triply charged **3** (Figure S14). Clearly, the size of the counterions does not measurably influence the collision cross-sections of large supramolecular assemblies. Hence, it must be their charge that causes the CCS changes discussed above. We will address this issue in detail in a new study concerning metallomacrocycles of many different sizes (up to decamer).

As mentioned earlier, the observation of intact hexameric (cyclic or linear) ions only in the MALDI mass spectrum of **3** indicates a stronger coordinative bonding in the <tpy−Ru^{II}−tpy> than the <tpy−Fe^{II}−tpy> connectivity. The TWIM results provide more details about the relative stabilities of the three macrocycles.

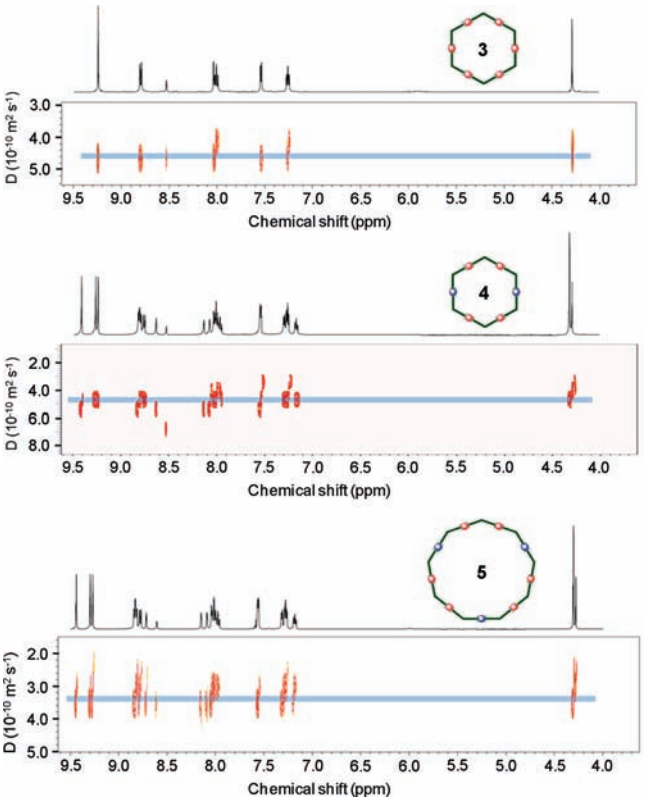

Figure 4. 2D DOSY NMR spectra of (a) hexamer **3**, (b) hexamer **4**, and (c) nonamer **5**.

Comparison of the relative intensities of the cyclic and extended linear components of hexamers **3** and **4**, Figure 1d, reveals that ca. 3.4% of the homonuclear macrocycle **3** ring-opened during ESI or ion mobility separation under the instrumental settings used. In contrast, heteronuclear **4**, which carries four Ru^{II} and two Fe^{II} ions, shows a higher amount (ca. 24%) of ring-opened isomer. Notably, an even higher fraction of nonamer **5** (ca. 36%) is converted to the linear isomer under the same conditions, consistent with the presence of more of the less stable <tpy−Fe^{II}−tpy> moieties (three) in this macrocyclic complex. Note that the percentages of linear structures given should be considered as lower limits, as any ring-like linear structures formed would overlap with the macrocyclic architectures. According to the modeling data, however, the population of ring-like linear conformers is much smaller than the population of extended linear conformers, especially for **3** and **4** (cf., Figures S11−S13). Hence, the conclusion that a larger number of <tpy−Fe^{II}−tpy> units in the macrocycle increases the efficiency of ring-opening remains valid. Ring-opening could occur while the ions travel through the lenses connecting the ESI source with the mass analyzers and/or in the TWIM region due to the internal energy imparted by the traveling wave during ion mobility separations;[50,96] irrespective of the cause, the extent of such reactions unveils insight about the intrinsic stabilities and reactivities of the systems being separated.

The lens and traveling wave parameters used to acquire the discussed TWIM data (see Experimental Section) maximized the sensitivity; however, parameters that sharply minimize isomerization and dissociation of the ions en route from the ion source to the detector can also be selected, at the expense of sensitivity. This is demonstrated for complex **3** in Figure S15; under mild

Table 2. Diffusion Coefficients, Hydrodynamic Radii, and Modeled Radii of Metallomacrocycles 3−5

complex	r_{CS} (exp) [nm][a]	D [10^{-10} m^2s^{-1}][b]	r_H (exp) [nm][c]	r_{inner} (calcd) [nm][d]	r_{outer} (calcd) [nm][d]	r_{mean} (calcd) [nm][d]
3	1.56	4.57	1.30	0.98	1.77	1.38
4	1.56	4.51	1.32	0.94	1.74	1.34
5	1.85	3.31	1.80	1.47	2.31	1.89

[a] r_{CS} (exp) is the radius of a circular area equal to the experimental collision cross-section; r_{CS} (exp) = [cross-section (exp)/π]$^{0.5}$. [b] Diffusion coefficient, deduced from the 2D DOSY NMR experiments conducted in CD_3CN at 298 K. [c] Hydrodynamic radii calculated via the Stokes−Einstein equation $D = k_BT/6\pi\eta r_H$ (k_B, Boltzmann constant; T, absolute temperature; η = 0.367 mPa·s, viscosity of CD_3CN at 298 K).[102] [d] Radii r_{inner} and r_{outer} calculated from the energy-minimized structures; $r_{mean} = (r_{inner} + r_{outer})/2$.

ESI and TWIM conditions, the drift time distributions of charge states 3+ to 7+ show only one sharp peak, arising from the macrocyclic architecture (cf., Figure S15). This result provides further evidence that the metallomacrocycles studied can survive intact while traveling from the ambient conditions of the ESI source to the vacuum system of the mass spectrometer and through the TWIM region.

2D DOSY NMR spectroscopy has been widely used to characterize supramacromolecules and monitor self-assembly processes by correlating chemical resonances to diffusion coefficients in solution.[101] The DOSY NMR spectra of macrocycles **3**, **4**, and **5** (Figure 4) unambiguously reveal the presence of only one species in solution for each substance. The experimental diffusion coefficients derived from spectra measured in CD_3CN at 298 K are 4.57×10^{-10}, 4.51×10^{-10}, and 3.31×10^{-10} m^2/s for complexes **3**, **4**, and **5**, respectively. For each complex, the experimental hydrodynamic radius (r_H), calculated via the Stokes−Einstein equation, agrees very well with the mean value of the inner and outer radii obtained from the respective energy-minimized macrocyclic structure (Table 2). Thus, the 2D DOSY NMR and TWIM MS are in concert, with both methods providing clear evidence that the self-assembled complexes **3**, **4**, and **5** have cyclic architectures. Note that r_H should not be used to calculate collision cross-sections; r_H represents the radius of a hard sphere that diffuses at the same rate as the species examined. For not perfectly spherical species, r_H is smaller than the effective or rotational radius (established by rotation about the species' geometric center).[102] On the other hand, a collision cross-section, and the radius calculated from it (r_{CS}), describe an area involving an ion-neutral complex, which is associated with a radius larger than r_H, as confirmed by the data in Table 2.

CONCLUSIONS

A series of homo- and heteronuclear metallomacrocycles with <tpy−M^{II}−tpy> (M = Fe or Ru) connectivity has been synthesized and characterized by NMR spectroscopy and mass spectrometry. The successful generation of a nonamer, which is most likely derived from the initially formed kinetic products, demonstrates the feasibility of synthesizing larger rings through the use of longer linear oligomers. In the size characterization, both the solution-phase hydrodynamic radii obtained by DOSY NMR and the gas-phase cross-sections acquired from TWIM MS agreed reasonably well with the values predicted computationally for the macrocyclic architectures. Considering the difficulty of single crystal growth, ion mobility mass spectrometry and diffusion NMR offer an alternative approach for the characterization of supramacromolecules. Because of the dispersive nature and high sensitivity of MS-based analyses, ion mobility mass spectrometry could become a crucial tool for the unambiguous characterization of supramolecular structure and size, especially if highly purified samples or ample sample amounts, as generally necessary for NMR studies, are not available.

ASSOCIATED CONTENT

Supporting Information. ^{1}H and 2D COSY NMR data; calculated and measured isotope patterns for the various charge states observed in the ESI mass spectra of the metallomacrocycles; calibration curve used to determine collision cross-sections from measured drift times; UV−vis absorption maxima (λ_{max}) and extinction coefficients (molar absorptivities ε); annealing cycles of molecular modeling; plots of collision cross-sections against the corresponding relative energies for the macrocycles and their linear isomers; collision cross-sections calculated using the PA and EHSS methods; tandem mass spectrum of the hexameric Ru^{II} complex; ESI mass spectrum of the hexameric Ru^{II} complex under mild conditions. This material is available free of charge via the Internet at http://pubs.acs.org.

AUTHOR INFORMATION

Corresponding Author

wesdemiotis@uakron.edu; newkome@uakron.edu

Author Contributions

[§]These authors contributed equally.

ACKNOWLEDGMENT

We thank the NSF for generous financial support (grants CHE-0517909 and 1012636 to C.W., DMR-0705015 to G.R. N., and DMR-0821313 for the purchase of the MS instrumentation used in this study). We gratefully acknowledge the expertise of Dr. Mingming Guo, Solid State NMR Manager at The University of Akron, for his help with the 2D-DOSY NMR experiments.

REFERENCES

(1) Lehn, J.-M. *Supramolecular Chemistry: Concepts and Perspectives*; VCH: Weinheim, 1995.
(2) Hasenknopf, B.; Lehn, J.-M.; Kneisel, B. O.; Baum, G.; Fenske, D. *Angew. Chem., Int. Ed. Engl.* **1996**, *35*, 1838–1840.
(3) Hasenknopf, B.; Lehn, J.-M.; Boumediene, N.; Dupont-Gervais, A.; Van Dorsselaer, A.; Kneisel, B.; Fenske, D. *J. Am. Chem. Soc.* **1997**, *119*, 10956–10962.
(4) Lehn, J.-M. *Chem.—Eur. J.* **1999**, *5*, 2455–2463.
(5) Lehn, J.-M. *Science* **2002**, *295*, 2400–2403.
(6) Ruben, M.; Rojo, J.; Romero-Salguero, F. J.; Uppadine, L. H.; Lehn, J.-M. *Angew. Chem., Int. Ed.* **2004**, *43*, 3644–3662.
(7) Stefankiewicz, A. R.; Rogez, G.; Harrowfield, J.; Drillon, M.; Lehn., J.-M. *J. Chem. Soc., Dalton Trans.* **2009**, 5787–5802.

(8) Stadler, A. M.; Puntoriero, F.; Nastasi, F.; Campagna, S.; Lehn, J.-M. *Chem.—Eur. J.* **2010**, *16*, 5645–5660.
(9) Northrop, B. H.; Yang, H. B.; Stang, P. J. *Chem. Commun.* **2008**, *2008*, 5896–5908.
(10) Northrop, B. H.; Zheng, Y. R.; Chi, K. W.; Stang, P. J. *Acc. Chem. Res.* **2009**, *42*, 1554–1563.
(11) Ghosh, K.; Hu, J.; White, H. S.; Stang, P. J. *J. Am. Chem. Soc.* **2009**, *131*, 6695–6697.
(12) Lee, J.; Ghosh, K.; Stang, P. J. *J. Am. Chem. Soc.* **2009**, *131*, 12028–12029.
(13) Wang, M.; Zheng, Y. R.; Ghosh, K.; Stang, P. J. *J. Am. Chem. Soc.* **2010**, *132*, 6282–6283.
(14) Fujita, M.; Sasaki, O.; Mitsuhashi, T.; Fujita, T.; Yazaki, J.; Yamaguchi, K.; Ogura, K. *Chem. Commun.* **1996**, 1535–1536.
(15) Takeda, N.; Umemoto, K.; Yamaguchi, K.; Fujita, M. *Nature* **1999**, *398*, 794–796.
(16) Hiraoka, S.; Fujita, M. *J. Am. Chem. Soc.* **1999**, *121*, 10239–10240.
(17) Tominaga, M.; Suzuki, K.; Kawano, M.; Kusukawa, T.; Ozeki, T.; Sakamoto, S.; Yamaguchi, K.; Fujita, M. *Angew. Chem., Int. Ed.* **2004**, *43*, 5621–5625.
(18) Fujita, M.; Tominaga, M.; Hori, A.; Therrien, B. *Acc. Chem. Res.* **2005**, *38*, 371–380.
(19) Suzuki, K.; Kawano, M.; Fujita, M. *Angew. Chem., Int. Ed.* **2007**, *46*, 2819–2822.
(20) Yoshizawa, M.; Klosterman, J. K.; Fujita, M. *Angew. Chem., Int. Ed.* **2009**, *48*, 3418–3438.
(21) Sun, Q. F.; Iwasa, J.; Ogawa, D.; Ishido, Y.; Sato, S.; Ozeki, T.; Sei, Y.; Yamaguchi, K.; Fujita, M. *Science* **2010**, *328*, 1144–1147.
(22) Holliday, B. J.; Mirkin., C. A. *Angew. Chem., Int. Ed.* **2001**, *40*, 2022–2043.
(23) Gianneschi, N. C.; Masar, M. S.; Mirkin, C. A. *Acc. Chem. Res.* **2005**, *38*, 825–837.
(24) Oliveri, C. G.; Ulmann, P. A.; Wiester, M. J.; Mirkin, C. A. *Acc. Chem. Res.* **2008**, *41*, 1618–1629.
(25) Kumar, A.; Sun, S. S.; Lees, A. J. *Coord. Chem. Rev.* **2008**, *252*, 922–939.
(26) Constable, E. C. *Coord. Chem. Rev.* **2008**, *252*, 842–855.
(27) Lee, S. J.; Lin, W. *Acc. Chem. Res.* **2008**, *41*, 521–537.
(28) Lusby, P. J. *Annu. Rep. Prog. Chem., Sect. A: Inorg. Chem.* **2009**, *105*, 323–347.
(29) De, S.; Mahata, K.; Schmittel, M. *Chem. Soc. Rev.* **2010**, *39*, 1555–1575.
(30) Schweiger, M.; Seidel, S. R.; Arif, A. M.; Stang, P. J. *Angew. Chem., Int. Ed.* **2001**, *40*, 3467–3469.
(31) Lee, S. J.; Hu, A.; Lin, W. *J. Am. Chem. Soc.* **2002**, *124*, 12948–12949.
(32) Hwang, S.-H.; Moorefield, C. N.; Fronczek, F. R.; Lukoyanova, O.; Echegoyen, L.; Newkome, G. R. *Chem. Commun.* **2005**, 713–715.
(33) Megyes, T.; Jude, H.; Grosz, T.; Bako, I.; Radnai, T.; Tarkanyi, G.; Palinkas, G.; Stang, P. J. *J. Am. Chem. Soc.* **2005**, *127*, 10731–10738.
(34) Zangrado, E.; Casanova, M.; Alessio, E. *Chem. Rev.* **2008**, *108*, 4979–5013.
(35) Schmittel, M.; Mahata, K. *Inorg. Chem.* **2009**, *48*, 822–824.
(36) Fujita, M.; Yazaki, J.; Ogura, K. *J. Am. Chem. Soc.* **1990**, *112*, 5645–5647.
(37) Cotton, F. A.; Daniels, L. M.; Lin, C.; Murillo, C. A.; Yu, S.-Y. *J. Chem. Soc., Dalton Trans.* **2001**, 502–504.
(38) Gang, H.; Dong, G.; Chun-Ying, D.; Hong, M.; Qing-Jin, M. *New J. Chem.* **2002**, *26*, 1371–1377.
(39) Liu, X.; Stern, C. L.; Mirkin, C. A. *Organometallics* **2002**, *21*, 1017–1019.
(40) Sun, S.-S.; Anspach, J. A.; Lees, A. J. *Inorg. Chem.* **2002**, *41*, 1862–1869.
(41) Ghosh, S.; Mukherjee, P. S. *Inorg. Chem.* **2009**, *48*, 2605–2613.
(42) Hwang, S.-H.; Wang, P.; Moorefield, C. N.; Godinez, L. A.; Manriquez, J.; Bustos, E.; Newkome, G. R. *Chem. Commun.* **2005**, 4672–4674.
(43) Chan, Y.-T.; Moorefield, C. N.; Soler, M.; Newkome, G. R. *Chem.—Eur. J.* **2010**, *16*, 1768–1771.
(44) Stang, P. J.; Persky, N. E.; Manna, J. *J. Am. Chem. Soc.* **1997**, *119*, 4777–4778.
(45) Newkome, G. R.; Cho, T. J.; Moorefield, C. N.; Baker, G. R.; Saunders, M. J.; Cush, R.; Russo, P. S. *Angew. Chem., Int. Ed.* **1999**, *38*, 3717–3721.
(46) Newkome, G. R.; Cho, T. J.; Moorefield, C. N.; Cush, R.; Russo, P. S.; Godinez, L. A.; Saunders, M. J; Mohapatra, P. *Chem.—Eur. J.* **2002**, *8*, 2946–2954.
(47) Newkome, G. R.; Cho, T. J.; Moorefield, C. N.; Mohapatra, P.; Godinez, L. A. *Chem.—Eur. J.* **2004**, *10*, 1493–1500.
(48) Halper, S. R.; Cohen, S. M. *Angew. Chem., Int. Ed.* **2004**, *43*, 2385–2388.
(49) Halper, S. R.; Cohen, S. M. *Inorg. Chem.* **2005**, *44*, 4139–4141.
(50) Chan, Y.-T.; Li, X.; Soler, M.; Wang, J. L.; Wesdemiotis, C.; Newkome, G. R. *J. Am. Chem. Soc.* **2009**, *131*, 16395–16397.
(51) Jones, P. L.; Byrom, K. J.; Jeffey, J. C.; McCleverty, J. A.; Ward, M. D. *Chem. Commun.* **1997**, 1361–1362.
(52) Grossmann, B.; Heinze, J.; Herdtweck, E.; Noth, H.; Schwenk, M.; Wachter, W.; Weber, W. *Angew. Chem., Int. Ed.* **1997**, *36*, 387–389.
(53) Takahashi, R.; Kobuke, Y. *J. Am. Chem. Soc.* **2003**, *125*, 2372–2373.
(54) Jiang, H.; Lin, W. *J. Am. Chem. Soc.* **2003**, *125*, 8084–8085.
(55) Jiang, H.; Lin, W. *J. Am. Chem. Soc.* **2004**, *126*, 7426–7427.
(56) Shoji, O.; Okada, S.; Satake, A.; Kobuke, Y. *J. Am. Chem. Soc.* **2005**, *127*, 2201–2210.
(57) Jiang, H.; Lin, W. *J. Am. Chem. Soc.* **2006**, *128*, 11286–11297.
(58) Sakamoto, S.; Fujita, M.; Kim, K.; Yamaguchi, K. *Tetrahedron* **2000**, *56*, 955–964.
(59) Schalley, C. A.; Muller, T.; Linnartz, P.; Witt, M.; Schafer, M.; Lutzen, A. *Chem.—Eur. J.* **2002**, *8*, 3538–3551.
(60) Engeser, M.; Rang, A.; Ferrer, M.; Gutierrez, A.; Baytekin, H. T.; Schalley, C. A. *Int. J. Mass Spectrom.* **2006**, *255−256*, 185–194.
(61) Wang, P.; Newkome, G. R.; Wesdemiotis, C. *Int. J. Mass Spectrom.* **2006**, *255−256*, 86–92.
(62) Sato, S.; Ishido, Y.; Fujita, M. *J. Am. Chem. Soc.* **2009**, *131*, 6064–6065.
(63) Jiang, W.; Schafer, A.; Mohr, P. C.; Schalley, C. A. *J. Am. Chem. Soc.* **2010**, *132*, 2309–2320.
(64) Ren, X.; Sun, B.; Tsai, C.-C.; Tu, Y.; Leng, S.; Li, K.; Kang, Z.; Van Horn, R. M.; Li, X.; Zhu, M.; Wesdemiotis, C.; Zhang, W.-B.; Cheng, S. Z. D. *J. Phys. Chem. B* **2010**, *114*, 4802–4810.
(65) Perera, S.; Li, X.; Soler, M.; Schultz, A.; Wesdemiotis, C.; Moorefield, C. N.; Newkome, G. R. *Angew. Chem., Int. Ed.* **2010**, *49*, 6539–6544.
(66) Brocker, E. R.; Anderson, S. E.; Northrop, B. H.; Stang, P. J; Bowers, M. T. *J. Am. Chem. Soc.* **2010**, *132*, 13486–13494.
(67) Li, X.; Chan, Y.-T.; Newkome, G. R.; Wesdemiotis, C. *Anal. Chem.* **2011**, *83*, 1284–1290.
(68) Bowers, M. T.; Kemper, P. R.; von Helden, G.; van Koppen, P. A. M. *Science* **1993**, *260*, 1446–1451.
(69) Clemmer, D. E.; Jarrold, M. F. *J. Mass Spectrom.* **1997**, *32*, 577–592.
(70) Hoaglund-Hyzer, C. S.; Counterman, A. E.; Clemmer, D. E. *Chem. Rev.* **1999**, *99*, 3027–3079.
(71) Verbeck, G. F.; Ruotolo, B. T.; Sawyer, H. A.; Gillig, K. J.; Russell, D. H. *J. Biomol. Tech.* **2002**, *13*, 56–61.
(72) Trimpin, S.; Plasencia, D. I.; Clemmer, D. E. *Anal. Chem.* **2007**, *79*, 7965–7974.
(73) Kanu, A. B.; Dwivedi, P.; Tam, M.; Matz, L.; Hill, H. H. *J. Mass Spectrom.* **2008**, *43*, 1–22.
(74) Ruotolo, B. T.; Benesch, J. L. P.; Sandercock, A. M.; Hyung, S. J.; Robinson, C. V. *Nat. Protocols* **2008**, *3*, 1139–1152.
(75) Fenn, L. S.; McLean, J. A. *Anal. Bioanal. Chem.* **2008**, *391*, 905–909.
(76) Trimpin, S.; Clemmer, D. E. *Anal. Chem.* **2008**, *80*, 9073–9083.

(77) Uetrecht, C.; Versluis, C.; Watts, N. R.; Wingfield, P. T.; Steven, A. C.; Heck, A. J. R. *Angew. Chem., Int. Ed.* **2008**, *47*, 6247–6251.
(78) Scarff, C. A.; Thalassinos, K.; Hilton, G. R.; Scrivens, J. H. *Rapid Commun. Mass Spectrom.* **2008**, *22*, 3297–3304.
(79) Van Duijn, E.; Barendregt, A.; Synowsky, S.; Versluis, C.; Heck, A. J. R. *J. Am. Chem. Soc.* **2009**, *131*, 1452–1459.
(80) Hilton, G. R.; Thalassinos, K.; Grabenauer, M.; Sanghera, N.; Slade, S. E.; Wyttenbach, T.; Robinson, P. J.; Pinheiro, T. J. T.; Bowers, M. T.; Scrivens, J. H. *J. Am. Soc. Mass Spectrom.* **2010**, *21*, 845–854.
(81) Giles, K.; Pringle, S. D.; Worthington, K. R.; Little, D.; Wildgoose, J. L.; Bateman, R. H. *Rapid Commun. Mass Spectrom.* **2004**, *18*, 2401–2414.
(82) Pringle, S. D.; Giles, K.; Wildgoose, J. L.; Williams, J. P.; Slade, S. E.; Thalassinos, K.; Bateman, R. H.; Bowers, M. T.; Scrivens, J. H. *Int. J. Mass Spectrom.* **2007**, *261*, 1–12.
(83) Thalassinos, K.; Grabenauer, M.; Slade, S. E.; Hilton, G. R.; Bowers, M. T.; Scrivens, J. H. *Anal. Chem.* **2009**, *81*, 248–254.
(84) Fernandez-Lima, F. A.; Blasé, R. C.; Russell, D. H. *Int. J. Mass Spectrom.* **2010**, *298*, 111–118.
(85) http://www.indiana.edu/~clemmer/Research/cross%20section%20database/Proteins/protein_cs.htm (accessed April 5, 2010).
(86) von Helden, G.; Hsu, M.-T.; Gotts, N.; Bowers, M. T. *J. Phys. Chem.* **1997**, *93*, 8182–8192.
(87) http://www.indiana.edu/~nano/software.html (accessed December 21, 2010).
(88) Shvartsburg, A. A.; Jarrold, M. F. *Chem. Phys. Lett.* **1996**, *261*, 86–91.
(89) Mesleh, M. F.; Hunter, J. M.; Shvartsburg, A. A.; Schatz, G. C.; Jarrold, M. F. *J. Phys. Chem.* **1996**, *100*, 16082–16086.
(90) Gunes, K.; Isayev, A. I.; Li, X.; Wesdemiotis, C. *Polymer* **2010**, *51*, 1071–1081.
(91) Wang, P.; Moorefield, C. N.; Newkome, G. R. *Org. Lett.* **2004**, *6*, 1197–1200.
(92) Evans, I. P.; Spencer, E. A.; Wilkinson, G. J. *Chem. Soc., Dalton Trans.* **1973**, 204–209.
(93) Meier, M. A. R.; Lohmeijer, B. G. G.; Schubert, U. S. *J. Mass Spectrom.* **2003**, *38*, 510–516.
(94) Bazzicalupi, C.; Bencini, A.; Bianchi, A.; Danesi, A.; Faggi, E.; Giorgi, C.; Santarelli, S.; Valtancoli, B. *Coord. Chem. Rev.* **2008**, *252*, 1052–1068.
(95) Schubert, U. S.; Hofmeier, H.; Newkome, G. R. *Modern Terpyridine Chemistry*, Weinheim, Wiley-VCH, 2006.
(96) Shvartsburg, A. A.; Smith, R. D. *Anal. Chem.* **2007**, *79*, 1523–1528.
(97) Wyttenbach, T.; Gidden, J.; Bowers, M. T. *In Ion Mobility Spectrometry-Mass Spectrometry*; Wilkins, C. E.; Trimpin, S., Eds.; CRC Press: Boca Raton, FL, 2011; Chapter 1, pp 3−30.
(98) Freeke, J.; Robinson, C. V.; Ruotolo, B. T. *Int. J. Mass Spectrom.* **2010**, *298*, 91–98.
(99) Seo, Y.; Schenauer, M. R.; Leary, J. A. *Int. J. Mass Spectrom.* **2011**, *303*, 191–198.
(100) Weiland, T.; Troff, R. W.; Saxell, H.; Rissanen, K.; Schalley, C. A. *Inorg. Chem.* **2008**, *47*, 7588–7598.
(101) Cohen, Y.; Avram, L.; Frish, L. *Angew. Chem., Int. Ed.* **2005**, *44*, 520–554.
(102) Lee, H.; Venable, R. M.; MacKerrell, A. D., Jr.; Pastor, R. W. *Biophys. J.* **2008**, *95*, 1590–1599.